Sudan University of Science and Technology
College of graduate Studies

Spectral Quasi-Linearisation Method for Solving Nonlinear ODEs Governing Some Types of Fluid Flow

طريقة SQLM لحل المعادلات التفاضلية العادية اللاخطيه التى تصف بعض من انواع سريان المائع

A thesis Submitted in Partial Fulfilment for the Degree of M.Sc in Mathematics

By

Mohamed Mostafa Alhaj Alamin Mostafa

Supervisor

Dr. Abdallah Habila Ali Kaitan

March 2016

ABSTRACT

In this thesis we study the spectral quasi-linearisation method ($SQLM$) and its applications on different types of nonlinear systems of ordinary differential equations. In chapter1 and chapter2 we present a literature review and details of the method of solution respectively. In chapter 3, we present a study of the convective heat transfer over inverted cone. The system of equations which governed the flow has been converted into a one equation then, we solve it using the spectral quasi-linearisation method. Also the effects of the power-law index parameter on the velocity, temperature profiles are determined. In chapter 4, we investigate the problem of nano-fluid flow over a wavy surface with non-controllable nanoparticle flux at the boundary. We solve the governing differential equations numerically by using the SQLM. The results presented in this study were shown graphically and in tabular form. The effects of the governing parameters namely the Local Rayleigh number, the buoyancy ratio, the Brownian motion parameter, the thermophoresis parameter and the local Lewis number are determined. The analysis of residual error and accuracy of the method are carried out.

المستخلص

فى هذا البحث قمنا بدراسة SQLM وتطبيقاتها على انواع مختلفة من انظمة المعادلات التفاضليه اللاخطية.

فى الباب الاول والثانى قدمنا تفاصيل عن نشاة طريقة SQLM واستخدامها فى الحل .

فى الباب الثالث قمنا بدراسه الحمل الحرارى وانتقاله داخل المخروط ونظام المعادلات التى تتحكم فى المائع قمنا بتحويلها فى معادلة واحدة، ثم قمنا بحلها باستخدام SQLM . تمت دراسة تأثير معامل بورلو على السرعة والحرارة.

فى الباب الرابع تحققنا من مشكلة تدفق المائع النانوى علي سطح متموج مع فيض من الجزيئات الخارجة عن السيطرة على الحدود وقمنا بعرض نتائج الدراسة في شكل جداول ورسومات. تم تحديد تأثيرات الوسائط التى توصف المائع مثل عدد رايليا المحلى، نسبة بيونسي، وسيط براون للحركة، وسيط مورفس الحرارى ورقم لويس. تم تحليل حد الخطأ والدقه لهذه الطريقة.

Contents

List of Tables

List of Figures

Chapter 1

Introduction

Differential equations arise in a number of physical problems, such as fluid flow, heat transfer, and biological processes. Finding solutions of the differential equations plays a crucial role in understanding the behavior of these problems. Mostly, the differential equations modeling real-life problems are nonlinear and complex to solve exactly and hence various analytical and numerical methods have been employed to approximate the solutions of these problems. One of the recent these methods is the spectral quasi-linearisation method which has been extended by Motsa [18] from the QLM. The classical method of quasi-linearization offers an approach for obtaining approximate solutions to nonlinear equations, the general properties of the QLM, particulary it's fast convergence, monotonicity and numerical stability are analyzed and illustrated on different physical problems. In a series of papers,[16] and [12] the possibility of applying a very powerful approximation technique called the quasi-linearization method to physical problems has been discussed. The QLM is designed to confront the nonlinear aspects of physical processes, the reason for the sparse use of the QLM in physics is that the convergence of the method has been proven only under rather restrictive conditions, which generally are not fulfilled physical applications. The quasi-linearization approach was introduced by Kalaba [13] and Bellman [2] as a generalization of the Newton-Raphson method [3, 21] to solve individual or systems of nonlinear ordinary and partial differential equations, and rearrangement of the governing nonlinear equa-

tions in a Gauss-Seidel manner. Modern developments and application of QLM to different fields are given in [14], the spectral collocation method to integrate the decoupled system. Using the steps described for a general case by Motsa [18], the resulting sequence of equations is integrated using the Chebyshev spectral collocation method. On the other hand, in the SQLM, the governing nonlinear equations are linearized using the Newton-Raphson based quasi-linearization method QLM, developed by Bellman and Kalaba [2], and are then integrated using Chebyshev spectral collocation method. A sizeable body of literature now exists on the use of various finite difference based QLM schemes in boundary layer flows described by both nonlinear ODEs and PDEs. Spectral method based quasi-linearisation schemes have been successfully applied to a range of fluid mechanics based ODEs model problems to be considerably more accurate than other traditional numerical methods such as finite difference and finite elements etc.

The structure of this research as follows: in Chapter 2, we gave the idea of the spectral quasi-linearization method SQLM, in Chapter 3 and 4, the governing ordinary differential equations are transformed into ordinary differential equations and then solved the main problem numerically by using SQLM. Then we have discussed the convergence of the SQLM and the effects of some physical parameters have been presented graphically and in tabular form.

Chapter 2

Spectral quasi-linearisation method (SQLM)

2.1 General governing equation system

Consider a system of m nonlinear ordinary differential equations in m unknowns functions $z_i(\eta)$ $i = 1, 2, 3, ..., m$ where η is the independent variable. The system can be written as a sum of it's linear $\mathbf{L}$ and nonlinear components $\mathbf{N}$ as

$$\mathbf{L}\left[z_1\left(\eta\right), z_2\left(\eta\right), ..., z_m\left(\eta\right)\right] + \mathbf{N}\left[z_1(\eta), z_2\left(\eta\right), ..., z_m(\eta)\right] = \mathbf{H}\left(\eta\right), \quad (\eta) \in (a, b), \tag{2.1}$$

subject to the boundary conditions

$$A_i\left[z_1\left(a\right), z_1\left(a\right), ..., z_m\left(a\right)\right] = K_{a,i}, \quad B_i\left[z_1\left(b\right), z_2\left(b\right), ..., z_m(b)\right] = K_{b,i}, \tag{2.2}$$

where A_i and B_i are linear operators and $K_{a,i}$ and $K_{b,i}$ are constants for $i = 1, 2, ..., m$. Define the vector Z_i to be the vector of the derivatives of the variable z_i with respect to the dependent variable η, that is

$$Z_i = \left[z_i^{(0)}, z_i^{(1)}, ..., z_i^{(n_i)}, \right], \tag{2.3}$$

where $z_i^{(0)} = z_i$, $z_i^{(p)}$ is the p^{th} derivative of z_i with respect to η and $n_i\,(i = 1, 2, .., m)$ is the highest derivative order of the variable z_i appearing in the system of equations.

In addition, we define $\mathbf{L}_i$ and $\mathbf{N}_i$ to be the linear and nonlinear operators, respectively, that operate on the Z_i for $i = 1, 2, .., m$, with these definitions,equation (2.1) and (2.2) can be written as

$$\mathbf{L}_i\left[Z_1, Z_2, ...Z_m\right] + \mathbf{N}_i\left[Z_1, Z_2, ...Z_m\right] = \sum_{j=1}^{m}\sum_{p=0}^{n_i} \alpha_{i,j}^{[p]} z_j^{(p)} + \mathbf{N}_i\left[Z_1, Z_2, ...Z_m\right] = \mathbf{H}_i, \quad (2.4)$$

where $\alpha_{i,j}^{[p]}$ are the constant coefficient of $z_j^{(p)}$, the derivative of $z_j\,(j = 1, 2, ...m)$ that appears in the i^{th} equation for $i = 1, 2, ..., m$. Noting that, for each variable z_i in the derivatives in the boundary conditions can at most be one less than the highest derivative of z_i in the governing system (2.1) we define the vector $\tilde{\mathbf{Z}}_i$ to be the vector of the derivatives of the variable z_i with respect to the dependent variable η from 0 up to $n_i - 1$, that is

$$\tilde{\mathbf{Z}}_i = \left[z_i^{(0)}, z_i^{(1)}, ..., z_i^{(n_i-1)}\right], \quad (2.5)$$

The boundary conditions(2.2) can be written as

$$A_\nu\left[\tilde{\mathbf{Z}}_1(a), \tilde{\mathbf{Z}}_2(a), ..., \tilde{\mathbf{Z}}_m(a)\right] = \sum_{j=1}^{m}\sum_{p=0}^{n_j-1} \beta_{\nu,j}^{[p]} z_j^{(p)}\,(a) = Ka, \nu, \;\; \nu = 1, 2, ..., m_a, \quad (2.6)$$

$$B_\sigma\left[\tilde{\mathbf{Z}}_1(b), \tilde{\mathbf{Z}}_2(b), ..., \tilde{\mathbf{Z}}_m(b)\right] = \sum_{j=1}^{m}\sum_{p=0}^{n_j-1} \gamma_{\sigma,j}^{[p]} z_j^{(p)}\,(b) = Kb, \sigma, \;\; \sigma = 1, 2, ..., m_b, \quad (2.7)$$

where $\beta_{\nu,j}^{[p]}$ and $\gamma_{\sigma,j}^{[p]}$ are the constants of $z_j^{(p)}$ in the boundary conditions,and m_a, m_b, are the total number of prescribed boundary condition, at $x = a$ and $x = b$ respectively. We remark that the sum $m_a + m_b$ is equal to the sum of the highest orders of the derivatives corresponding to the dependent variable z_i,that is

$$m_a + m_b = \sum_{i=1}^{m} n_i, \quad (2.8)$$

2.2 Spectral Quasi-linearisation Method(SQLM)

Assume that the solution $z_i(\eta)$ of (2.4) at the $(r+1)$th iteration is $z_{i,r+1}$. If the solution at the previous iteration $z_{i,r}(\eta)$ is sufficiently close to $z_{i,r+1}$, the nonlinear component

$\mathbf{N}_i$ of the equation (2.4) can be linearised using one term Taylor series for multiple variable so that equation (2.4) can be approximated as.

$$\mathbf{L}_i\left[Z_{1,r+1},...,Z_{m,r+1}\right]+\mathbf{N}_i\left[...\right]+\sum_{j=1}^{m}\sum_{p=0}^{n_j}\left(z_{j,r+1}^{(p)}-z_{j,r}^{(p)}\right)\frac{\partial\mathbf{N}_i}{\partial z_j^{(p)}}\left[...\right]=\mathbf{H}_i(\eta), \tag{2.9}$$

subject to

$$\sum_{j=1}^{m}\sum_{p=0}^{n_j-1}\beta_{\nu,j}^{[p]}z_{j,r+1}^{[p]}(a)=0, \qquad \nu=1,2,..,m_a, \tag{2.10}$$

$$\sum_{j=1}^{m}\sum_{p=0}^{n_j-1}\gamma_{\sigma,j}^{[p]}z_{j,r+1}^{[p]}(b)=0, \qquad \nu=1,2,..,m_b, \tag{2.11}$$

where

$$\left[...\right]=\left[Z_{1,r},Z_{2,r},...,Z_{m,r}\right], \tag{2.12}$$

Equation (2.9) can be rewritten as

$$\mathbf{L}_i\left[Z_{1,r+1},...Z_{m,r+1}\right]+\sum_{j=1}^{m}\sum_{p=0}^{n_j}z_{j,r+1}^{(p)}\frac{\partial\mathbf{N}_i}{\partial z_j^{(p)}}[..]=\mathbf{H}_i(\eta)+\sum_{j=1}^{m}\sum_{p=0}^{n_j}z_{j,r}^{(p)}\frac{\partial\mathbf{N}_i}{\partial z_j^{(p)}}[..]-\mathbf{N}_i\left[..\right], \tag{2.13}$$

The iterative scheme (2.13) is called the spectral quasi-linearisation method (SQLM). The initial approximation $z_{j,0}(\eta)$, required to start the iteration scheme (2.13) is chosen to be a function that satisfies the boundary condition (2.2). As guide, the initial guess can be obtained as a solution of the linear part of (2.1) subject to the boundary condition (2.2) that is,we solve

$$\sum_{j=1}^{m}\sum_{p=0}^{n_j}\alpha_{i,j}^{[p]}z_{j,0}^{(p)}=\mathbf{H}_i(\eta), \tag{2.14}$$

subject to

$$\sum_{j=1}^{m}\sum_{p=0}^{n_j-1}\beta_{\nu,j}^{[p]}z_{j,0}^{(p)}(a)=K_{a,\nu}, \qquad \nu=1,2,...,m_a, \tag{2.15}$$

$$\sum_{j=1}^{m}\sum_{p=0}^{n_j-1}\gamma_{\sigma,j}^{[p]}z_{j,0}^{(p)}(b)=K_{b,\sigma}, \qquad \sigma=1,2,...,m_b, \tag{2.16}$$

2.3 Solution Method

To solve the iteration scheme (2.13) it is convenient to use the Chebyshev spectral collocation method. For brevity, we omit the details of the spectral methods, and refer interested readers to ([4, 24]). Before applying the spectral methods, it is convenient to transform the domain on which the governing equation is defined to the interval $[-1, 1]$ on which the spectral method can be implemented. We use the transformation $x = (b-a)(\tau+1)/2$ to map the interval $[a, b]$ to $[-1, 1]$. The basic idea behind the spectral collocation method is the introduction of a differentiation matrix $\mathbf{D}$ which is used to approximate the derivatives of the unknown variables $z_i(\eta)$ at the collocation points the matrix vector product.

$$\frac{dz_i}{d\eta} = \sum_{k=0}^{N} \mathbf{D}_{lk} z_i(\tau_k) = \mathbf{D}\mathbf{Z}_i, \qquad l = 0, 1, ...N, \tag{2.17}$$

where $N+1$ is the number of collocation points (grid points), $\mathbf{D} = 2D/(b-a)$ and $\mathbf{Z} = [z(\tau_0), z(\tau_1), ..., z(\tau_N)]^T$ is a vector function at the collocation points Higher order derivatives are obtained as powers of $\mathbf{D}$, that is

$$z_j^{(p)} = \mathbf{D}^p \mathbf{Z}_j, \tag{2.18}$$

The solution process is applied in two stages. First we determine the initial approximation $Z_{i,o}$ $(i = 1, 2, ..., m)$ then using the solution of the initial approximation, we solve the recursive iteration scheme (2.9). Applying the chebyshev spectral method on the initial approximation equations $(2.14 - 2.16)$ we obtain,

$$\sum_{j=1}^{m} \sum_{p=0}^{n_j} \alpha_{i,j}^{[p]} \mathbf{D}^p \mathbf{Z}_{j,0} = \mathbf{H}_i(\eta), \tag{2.19}$$

subject to

$$\sum_{j=1}^{m} \sum_{p=0}^{n_j-1} \beta_{\nu,j}^{[p]} \sum_{k=0}^{N} \mathbf{D}_{Nk}^p z_{j,0}(\tau_k) = K_{a,\nu} \qquad \nu = 1, 2, ..., m_a, \tag{2.20}$$

$$\sum_{j=1}^{m} \sum_{p=0}^{n_j-1} \gamma_{\sigma,j}^{[p]} \sum_{k=0}^{N} \mathbf{D}_{0k}^p z_{j,0}(\tau_k) = K_{b,\sigma} \qquad \sigma = 1, 2, ..., m_b, \tag{2.21}$$

Equations (2.19) can be written in matrix form as

$$\begin{bmatrix} A_{1,1} & A_{1,2} & .... & A_{1,m} \\ A_{2,1} & A_{2,2} & \dots & A_{2,m} \\ \vdots & \vdots & & \vdots \\ A_{m,1} & A_{m,2} & .... & A_{m,m} \end{bmatrix} \begin{bmatrix} \mathbf{Z}_{1,0} \\ \mathbf{Z}_{2,0} \\ \vdots \\ \mathbf{Z}_{m,0} \end{bmatrix} = \begin{bmatrix} \mathbf{H}_1 \\ \mathbf{H}_2 \\ \vdots \\ \mathbf{H}_m \end{bmatrix}, \tag{2.22}$$

where $\mathbf{Z}_{i,0}$ are the vectors of size $(N+1)\times 1$ and $A_{i,j}$ are $(N+1)\times(N+1)$ matrices which are respectively, define as

$$Z_{i,0} = [z_{i,0}(\tau_0), z_{i,0}(\tau_1), ..., z_{i,0}(\tau_N)] \tag{2.23}$$

Thus, the size of the coefficient matrix is $m(N+1)\times\ m(N+1)$ and the column vector on the right hand side has dimension $m\,(N+1)\times 1$. Applying the chebyshev spectral collocation on the recursive iteration scheme (2.13) gives

$$\sum_{j=1}^{m} \left[A_{i,j} + \Pi_{i,j}\right] \mathbf{Z}_{j,r+1} = \Phi_{i,r} \qquad i,j = 1,2,3,...,m, \tag{2.24}$$

where $\mathbf{Z}_{i,r+1} = [z_{i,r+1}(\tau_0), z_{i,r+1}(\tau_1), ..., z_{i,r+1}(\tau_N)]^T$, $A_{i,j}$ is as defined in (2.13) and $\Pi_{i,j}$ and $\Phi_{i,r}$ are given by

$$\Pi_{i,j} = \sum_{p=0}^{n_j} \mathbf{daig}\left[\frac{\partial N_i}{\partial z_j^{(p)}}\right] \mathbf{D}^p, \tag{2.25}$$

$$\Phi_{i,r} = H_i(\eta) + \sum_{j=1}^{m}\sum_{p=0}^{n_j} z_{j,r}^{(p)} \frac{\partial N_i}{\partial z_j^{(p)}} [....] - N_i\left[Z_{1,r}, Z_{2,r}, ..., Z_{m,r}\right], \tag{2.26}$$

respectively, where diag[...] means denote diagonal matrix. Defining $\Delta = A + \Pi$, we can write equation (2.24) in matrix form as

$$\begin{bmatrix} \Delta_{1,1} & \Delta_{1,2} & .... & \Delta_{1,m} \\ \Delta_{2,1} & \Delta_{2,2} & \dots & \Delta_{2,m} \\ \vdots & \vdots & & \vdots \\ \Delta_{m,1} & \Delta_{m,2} & .... & \Delta_{m,m} \end{bmatrix} \begin{bmatrix} \mathbf{Z}_{1,r+1} \\ \mathbf{Z}_{2,r+1} \\ \vdots \\ \mathbf{Z}_{m,r+1} \end{bmatrix} = \begin{bmatrix} \Phi_{1,r} \\ \Phi_{2,r} \\ \vdots \\ \Phi_{m,r} \end{bmatrix}, \tag{2.27}$$

where $\mathbf{Z}_{i,r}$,$\Phi_{i,r}$ are vectors of size $(N+1)\times 1$ and $\Delta_{i,j}$ are $(N+1)\times(N+1)$ matrices. starting from $Z_{i,0}$, the recursive sequence (2.27) is solved iteratively for $r = 0,1,2,3,....$

Chapter 3

Convective heat transfer over inverted Cone

3.1 Mathematical Formulation

Consider an inverted cone with semi-angle γ. We take the origin of the coordinate system to be at the vertex of the cone, the x-axis is the coordinate along the surface of the cone and y is the coordinate normal to the surface of the cone. The boundary layer develops over the heated frustum $x = x_0$. In terms of the stream function ψ defined by:

$$u = \frac{1}{r}\frac{\partial \psi}{\partial y},\ v = -\frac{1}{r}\frac{\partial \psi}{\partial x}, \tag{3.1}$$

the boundary layer equations are :

$$\frac{1}{r}\frac{\partial^2 \psi}{\partial^2 y} = \frac{g\beta k}{\nu}\frac{\partial T}{\partial y}, \tag{3.2}$$

$$\frac{1}{r}\left(\frac{\partial \psi}{\partial y}\frac{\partial T}{\partial x} - \frac{\partial \psi}{\partial x}\frac{\partial T}{\partial y}\right) = \alpha\frac{\partial^2 T}{\partial^2 y}. \tag{3.3}$$

For a thin boundary layer we have approximately $r = x\sin(\gamma)$. We suppose that either a power law of temperature of a power law of heat flux is prescribed on the frustum,where u and v are velocity vectors along x and y axes, x_0 distant of start point of cone from the vertex, ψ is stream function, β is expantion coefficient of the fluid, ν is

the Kinematic viscosity of the fluid, K is the permeability of the fluid-saturated porous medium, α is thermal diffusivity of the fluid-saturated porous medium, Accordingly, the boundary condition are:

$$\begin{aligned} &y \longrightarrow \infty : \qquad u = 0, T = T_\infty, \\ &y = 0\,, x_0 \leq x < \infty : u = 0 \text{ and either } T = T_w = T_\infty + (x - x_0)^\lambda\,, \\ &\text{or} \qquad q'' = -k\frac{\partial T}{\partial y}|_{y=0} = A\,(x - x_0)^\lambda\,, \qquad y = 0, \qquad x_0 \leq x < \infty. \end{aligned} \tag{3.4}$$

For the case of a full cone ($x_0 = 0$) a similarity solution exists. In the case of prescribe wall temperature, we let:

$$\psi = \alpha r Ra_x^{1/3} f(\eta), \qquad T - T_\infty = \frac{q''x}{k} Ra_x^{-1/3}\theta(\eta), \qquad \eta = \frac{y}{x} Ra_x^{1/3}, \tag{3.5}$$

where the Rayleigh number is based on heat flux ,

$$Ra_x = \frac{g\beta k\cos(\gamma) q'' x^2}{\nu\alpha k}, \qquad Tw - T_\infty = \frac{q''x}{k} Ra_x^{-1/3}. \tag{3.6}$$

The governing equations become

$$f' = \theta, \tag{3.7}$$

$$\theta'' + \left(\frac{\lambda + 5}{2}\right) f\theta' - \frac{2\lambda + 1}{3} f'\theta = 0, \tag{3.8}$$

subject to

$$f(0) = 0, \qquad \theta'(0) = -1, \qquad \theta(\infty) = 0, \tag{3.9}$$

finally from (3.7) and (3.9) we have

$$f''' + \left(\frac{\lambda + 5}{2}\right) ff'' - \left(\frac{2\lambda + 1}{3}\right) f'^2 = 0, \tag{3.10}$$

$$f(0) = 0, \qquad f''(0) = -1, \qquad f'(\infty) = 0. \tag{3.11}$$

The parameter of engineering interest in heat transport problems is the local Nusselt number which is defined as:

$$Nu_x = \frac{q_w x}{k(Tw - T_\infty)}, \tag{3.12}$$

From Equation (3.12), (3.5) and (3.6) the local Nusselt number is given by :

$$Nu_x = Ra_x^{1/3}\left[-\theta(0)\right], \tag{3.13}$$

3.2 Solution Method (SQLM)

The equation is expressed in terms of the similarity variable $\eta \in [0, \infty)$ and function $f(\eta)$ as

$$f''' + \left(\frac{\lambda+5}{2}\right) f f'' - \left(\frac{2\lambda+1}{3}\right) f'^2 = 0, \tag{3.14}$$

where the primes denote differentiation with respect to η. The nonlinear component

$$N_1 = f f'', \qquad N_2 = f'^2, \tag{3.15}$$

can be linearised using one term Taylor series for multiple variables so the approximation gives the following form

$$f f'' = f_r f''_{r+1} + f''_r f_{r+1} - f_r f''_r, \tag{3.16}$$

$$f'^2 = 2 f_r f'_{r+1} - f'^2_r \tag{3.17}$$

hence, we can rewrite equation (3.10) to give the following iteration scheme:

$$f'''_{r+1} + \left(\frac{\lambda+5}{2}\right)\left(f''_r f_{r+1} + f_r f''_{r+1}\right) - \left(\frac{2}{3}\right)(2\lambda+1)\left(f'_r f'_{r+1}\right) = \left(\frac{\lambda+5}{2}\right) f_r f''_r - \left(\frac{2\lambda+1}{3}\right) f'^2_r, \tag{3.18}$$

In the framework of the SQLM, (3.18) can be presented in the following form:

$$[\mathbf{A}]\,[f_{r+1}] = [\mathbf{R}_r]\,, \tag{3.19}$$

where $\mathbf{R}_r$ is a vector of size $(N+1) \times 1$ and $\mathbf{A}$ is $(N+1) \times (N+1)$ matrix defined as

$$\mathbf{A} = \mathbf{D}^3 + \frac{1}{2}(\lambda+5)\,\mathbf{diag}\,[f_r]\,\mathbf{D}^2 - \frac{2}{3}(2\lambda+1)\,\mathbf{diag}\,[f'_r]\,\mathbf{D} + \frac{1}{2}(\lambda+5)\,\mathbf{diag}[f''_r], \tag{3.20}$$

$$\mathbf{R}_r = \frac{1}{2}(\lambda+5)\, f_r f''_r - \frac{1}{3}(2\lambda+1)\, f'^2_r. \tag{3.21}$$

To impose the boundary conditions (3.9) in $\mathbf{A}$ and $\mathbf{R}$ it is better to use the matrix and vector forms as follows

$$\begin{bmatrix} D_{0,0} & D_{0,1} & \dots & D_{0,N-1} & D_{0,N} \\ & & \mathbf{A} & & \\ D^2_{N,0} & D^2_{N,1} & \dots & D^2_{N,N-1} & D^2_{N,N} \\ 0 & 0 & \dots & 0 & 1 \end{bmatrix} \begin{bmatrix} f_0 \\ \vdots \\ f_{N-1} \\ f_N \end{bmatrix} = \begin{bmatrix} 0 \\ R_1 \\ \vdots \\ 0 \end{bmatrix}, \tag{3.22}$$

Finally, the approximation solution of the original differential equations is obtained by solving the equation (3.19) as:

$$f_{r+1} = \tilde{\mathbf{A}}^{-1}\tilde{\mathbf{R}}, \tag{3.23}$$

where $\tilde{\mathbf{A}}$ and $\tilde{\mathbf{R}}$ are the modified matrices of $\mathbf{A}$ and $\mathbf{R}$ We define the following relative error formula using the infinity norm

$$E_{r,N,\eta_\infty} = \frac{\|\Delta_r - \Delta_{r-1}\|_\infty}{\|\Delta_{r-1}\|_\infty} \times 100. \tag{3.24}$$

The relative error depends on the iteration r, number of grid points (which is a value chosen to be large enough to numerically approximate infinity.

3.3 Results and discusition

The governing equations (3.2) and (3.3) are transformed into nonlinear ordinary differential equation (3.7) with the boundary conditions (3.11) and the resulting equation solved numerically using the SQLM. In order to verify the accuracy of our solution,

Table 3.1: Comparation between SQLM solution, HAM solution and numerical solution for $\theta(0)$ for various amount of λ.

λ	SQLM					Sohouli et al.[23]	Numerical
	ord 4	ord 5	ord 6	ord 7	ord 8		
0	0.94705	0.94751	0.94759	0.94760	0.94760	0.94783	0.94760
$\frac{1}{4}$	0.91080	0.91120	0.91127	0.91128	0.91128	0.91119	0.91130
$\frac{1}{3}$	0.89984	0.90023	0.90029	0.90030	0.90031	0.90103	0.90030
$\frac{1}{2}$	0.85178	0.87973	0.87979	0.87980	0.87980	0.87964	0.87980
$\frac{3}{4}$	0.85178	0.85209	0.85214	0.85215	0.85215	0.85242	0.85220
1	0.82727	0.82755	0.82755	0.82760	0.82761	0.82726	0.82760

the comparison of surface temperature obtained by the SQLM with those reported by Sohouli et al.[23] is shown in Table 3.1. It is clear that the SQLM results in a good

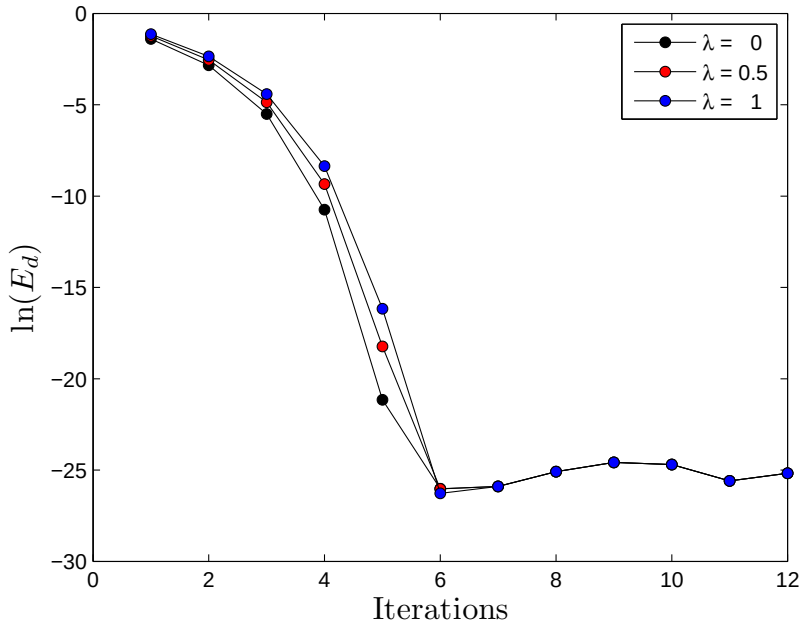

Figure 3.1: Logarithm of the SQLM error for different values of λ

agreement in order of accuracy and convergence. However the snap shot of the surface temperature values to demonstrate the effect of increasing the power law parameter λ. On the convergence rate of the SQLM, in general, with few iterations of the SQLM are sufficient to give a match with the numerical results up to five decimal places. In order to determine the evolution of the boundary layer flow properties and the convergence analysis, numerical solution determined with $\eta_\infty = 20$, $N = 100$. Fig. 3.1 shows the variation of the error against the iterations of the SQLM scheme. It can be seen that the iteration scheme takes about six or seven iterations to converge fully. Beyond the point where full convergence is reached, error norm levels off and does not improve with an increase in the number of iterations. Fig. 3.2 shows the effects of the power-law index parameter λ on the velocity profile. It is evident the dimensionless velocity decreases with increasing in the power-law index parameter. Fig. 3.3 illustrates the variation of the dimensionless temperature profile $\theta(\eta)$ for selected values of λ. Increasing λ contributes to reducing the temperature profile.

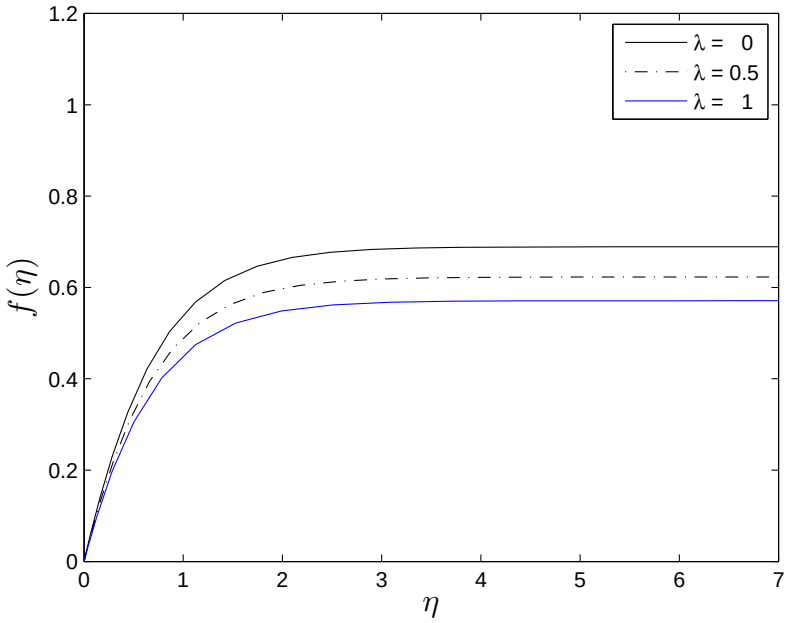

Figure 3.2: The velocity profile $f(\eta)$ for different values of λ

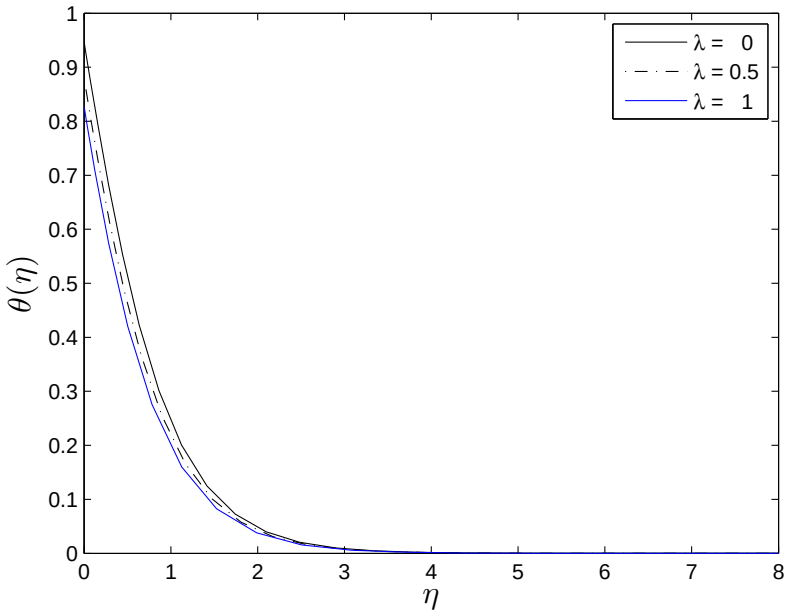

Figure 3.3: The dimensionless temperature $\theta(\eta)$ for different values of λ

Chapter 4

Nano-fluid flow over a wavy surface with non-controllable nanoparticle flux at the boundary

4.1 Introduction

Most common fluids such as water, ethylene, glycol, toluene or oil generally have poor heat transfer characteristics owing to their low thermal conductivity. A recent technique to improve the thermal conductivity of these fluids is to suspend nano-sized metallic particles such as aluminum, titanium, gold, copper, iron or their oxides in the fluid to enhance its thermal properties, Choi [7]. The enhancement of thermal conductivity in nanofluids has been studied by, among others, Kakac and Pramuanjaroenkij [11], Choi et al. [8], Masuda et al. [17], Eapen et al. [9] and Fan and Wang [10]. Nield and Kuznetsov [19] analyzed the behaviour of boundary layer flow on the Chen-Minkowycz problem in a porous layer saturated with a nanofluid. Nield and Kuznetsov [20] investigated thermal instability in a porous medium saturated with nanofluid using the Brinkman model. The model incorporated the effects of Brownian motion and thermophoresis of nanoparticles. They found that the critical thermal Rayleigh

number can be reduced or increased by a substantial amount depending on whether the nanoparticle distribution is top-heavy or bottom-heavy. Aziz et al. [1] studied steady boundary layer flow past a horizontal flat plate embedded in a porous medium filled with a water-based nanofluid containing gyrotactic microorganisms. Cheng [6] investigated the behaviour of boundary layer flow over a horizontal cylinder of elliptic cross section in a porous medium saturated with a nanofluid. Chamkha et al. [5] investigated the non-similar solutions for natural convective boundary layer flow over a sphere embedded in a porous medium saturated with a nanofluid.

4.2 Mathematical Formulation

We consider a laminar flow of a nanofluid along a vertical sinusoidally wavy surface embedded in a porous medium governed by $\hat{y} = \hat{a}\sin(\hat{x}/l)$ (see Rees and Pop) with constant wall temperature and nanoparticle concentration T_w and $\hat{\phi}_w$ which are higher than ambient values T_∞ and $\hat{\phi}_\infty$ respectively. Using two-dimensional cartesian coordinates $(\hat{x}, \hat{y})$, define the characteristic length scale associated with the sinusoidal waves to be l and the amplitude of the surface wave is $\hat{a}$, the governing equations are

$$\frac{\partial u}{\partial \hat{x}} + \frac{\partial v}{\partial \hat{y}} = 0, \tag{4.1}$$

$$\frac{\mu}{\mathtt{K}}\frac{\partial u}{\partial \hat{y}} = \frac{\partial \mathtt{p}}{\partial \hat{x}} + \left[(1-\hat{\phi})\rho_{f_\infty}\beta(T-T_\infty) - (\rho_{\mathtt{p}} - \rho_{f_\infty})(\hat{\phi}-\hat{\phi}_\infty)\right]\mathrm{g}, \tag{4.2}$$

$$\frac{\mu}{\mathtt{K}}\frac{\partial v}{\partial \hat{x}} = \frac{\partial \mathrm{p}}{\partial \hat{y}}, \tag{4.3}$$

$$u\frac{\partial T}{\partial \hat{x}} + v\frac{\partial T}{\partial \hat{y}} = \alpha_{\mathtt{m}}\left(\frac{\partial^2 T}{\partial \hat{x}^2} + \frac{\partial^2 T}{\partial \hat{y}^2}\right) + \tau\left[\mathtt{D_B}\left(\frac{\partial \hat{\phi}}{\partial \hat{x}}\frac{\partial T}{\partial \hat{x}} + \frac{\partial \hat{\phi}}{\partial \hat{y}}\frac{\partial T}{\partial \hat{y}}\right) + \frac{\mathtt{D_T}}{\mathtt{T}_\infty}\left(\left(\frac{\partial T}{\partial \hat{x}}\right)^2 + \left(\frac{\partial T}{\partial \hat{y}}\right)^2\right)\right], \tag{4.4}$$

$$u\frac{\partial \hat{\phi}}{\partial \hat{x}} + v\frac{\partial \hat{\phi}}{\partial \hat{y}} = \mathtt{D_B}\left(\frac{\partial^2 \hat{\phi}}{\partial \hat{x}^2} + \frac{\partial^2 \hat{\phi}}{\partial \hat{y}^2}\right) + \frac{\mathtt{D_T}}{\mathtt{T}_\infty}\left(\frac{\partial^2 T}{\partial \hat{x}^2} + \frac{\partial^2 T}{\partial \hat{y}^2}\right), \tag{4.5}$$

subject to the boundary conditions

$$v = 0,\ T = T_{\mathtt{w}},\ D_B\frac{\partial \hat{\phi}}{\partial \hat{y}} + \frac{D_T}{T_\infty}\frac{\partial T}{\partial \hat{y}} = 0 \text{ on } \hat{y} = a\sin\hat{x}, \tag{4.6}$$

$$u \to 0,\ T \to T_\infty,\ \hat{\phi} = \hat{\phi}_\infty \quad \text{on} \quad \hat{y} \to \infty, \tag{4.7}$$

where u and v are the velocity components along the $\hat{x}$ and $\hat{y}$ directions, respectively, $\mathbf{g}$ is the acceleration due to gravity, K is the permeability of the porous medium, ρ_f is the base fluid density, ρ_p is the nanoparticle density, μ is the absolute viscosity of the base fluid, α_m is the thermal diffusivity of the porous medium, T the fluid temperature of the fluid, $\hat{\phi}$ is the nanoparticle volume fraction, p is the pressure of the fluid, D_B is the Brownian diffusion coefficient, D_T is thermophoresis diffusion coefficient, $(\rho c)_f$ and $(\rho c)_p$ are the heat capacity of the fluid and the effective heat capacity of the nanoparticle material respectively, $\tau = \frac{(\rho c)_f}{(\rho c)_p}$ is the ratio between the effective heat capacity of the nanoparticle material and heat capacity of the fluid.

We introduce the following similarity transformations

$$x = \hat{x}/l,\ y = \hat{y}/l,\ \psi = \hat{\psi}/\alpha_m,\ \theta = (T - T_\infty)/(T_\mathtt{w} - T_\infty),$$
$$\Phi = (\hat{\phi} - \hat{\phi}_\infty)/\hat{\phi}_\infty, \tag{4.8}$$

where $\hat{\psi}$ can be define by $u = \frac{\partial \psi}{\partial \hat{y}}$ and $v = -\frac{\partial \psi}{\partial \hat{x}}$. Substituting (4.8) into (4.2)-(4.5) yields

$$\frac{\partial^2 \psi}{\partial x^2} + \frac{\partial^2 \psi}{\partial y^2} = \mathtt{Ra}\left[\frac{\partial \Theta}{\partial y} - \mathtt{Nr}\frac{\partial \Phi}{\partial y}\right], \tag{4.9}$$

$$\frac{\partial \psi}{\partial y}\frac{\partial \Theta}{\partial x} - \frac{\partial \psi}{\partial x}\frac{\partial \Theta}{\partial y} = \left(\frac{\partial^2 \Theta}{\partial x^2} + \frac{\partial^2 \Theta}{\partial y^2}\right) + \mathtt{Nb}\left(\frac{\partial \Phi}{\partial x}\frac{\partial \Theta}{\partial x} + \frac{\partial \Phi}{\partial y}\frac{\partial \Theta}{\partial y}\right) + \mathtt{Nt}\left[\left(\frac{\partial \Theta}{\partial x}\right)^2 + \left(\frac{\partial \Theta}{\partial y}\right)^2\right], \tag{4.10}$$

$$\mathtt{Le}\left[\frac{\partial \psi}{\partial y}\frac{\partial \Phi}{\partial x} - \frac{\partial \psi}{\partial x}\frac{\partial \Phi}{\partial y}\right] = \left(\frac{\partial^2 \Phi}{\partial x^2} + \frac{\partial^2 \Phi}{\partial y^2}\right) + \frac{\mathtt{Nt}}{\mathtt{Nb}}\left(\frac{\partial^2 \Theta}{\partial x^2} + \frac{\partial^2 \Theta}{\partial y^2}\right), \tag{4.11}$$

with the boundary conditions

$$\frac{\partial \psi}{\partial x} = 0,\ \Theta = 1,\ N_b\frac{\partial \Phi}{\partial y} + N_t\frac{\partial \Theta}{\partial y} = 0, \quad \text{on} \quad y = a\sin x, \tag{4.12}$$

$$\frac{\partial \psi}{\partial y} \to 0,\ \theta \to 0,\ \Phi \to 0 \quad \text{when} \quad y \to \infty. \tag{4.13}$$

The parameters of primary interest are the Local Rayleigh number $\mathtt{Ra}$, the buoyancy ratio $\mathtt{Nr}$, the Brownian motion parameter $\mathtt{Nb}$, the thermophoresis parameter $\mathtt{Nt}$, the

local Lewis number Le. These parameters are defined as

$$\mathtt{Ra} = \frac{(1-\hat{\phi}_\infty)\rho_f \mathrm{g} K\beta\Delta T H}{\alpha_m \mu},\ \mathtt{Nr} = \frac{(\rho_p-\rho_f)K\Delta\hat{\phi}}{\rho_f\beta(1-\hat{\phi}_\infty)\Delta T},\ \mathtt{Nb} = \frac{\tau D_B \Delta C}{\alpha_m T_c},$$
$$\mathtt{Nt} = \frac{\tau D_T \Delta T}{\alpha_m},\ \mathtt{Le} = \frac{\alpha_m}{D_B}.$$

The heat and nanoparticle volume fraction transfer coefficients are described by the Nusselt number Nu and the Sherwood number Sh are defined as

$$Nu = \frac{-xq_{\mathrm{w}}}{\alpha_m(T_{\mathrm{w}}-T_\infty)},\ Sh = \frac{-xq_m}{D_B(\hat{\phi}_{\mathrm{w}}-\hat{\phi}_\infty)}$$

where the heat flux q_{w} and the nanoparticle flux, q_m are given by.

$$q_{\mathrm{w}} = -\alpha_m \left.\frac{\partial T}{\partial y}\right|_{y=0} \quad \text{and} \quad q_m = -D_B \left.\frac{\partial \hat{\phi}}{\partial y}\right|_{y=0}.$$

The non-dimensional form of the Nusselt number and Sherwood number are

$$Nu_x/Re^{\frac{1}{2}} = -\Theta'(0),\ Shw_x/Re^{\frac{1}{2}} = -\Phi'(0),$$

where $Re_x = \frac{Ux}{\nu}$ is the local Reynolds number. following Rees and Pop [22], and Narayana and Sibanda [15], we assume that Rayleigh number is large, so that our model can define the free convection within a narrow region whose cross-stream width is substantially smaller than the $O(1)$ amplitude of the surface waves. Using the non-dimensional variables,

$$x = \xi, \quad y = \xi^{1/2} Ra^{-1/2}\eta + a\sin(x), \quad \Psi = Ra^{1/2}\psi, \tag{4.14}$$

for the largest values of Rayleigh number $Ra \to \infty$, we can write the system (4.9) - (4.11),

$$\left(1+a^2\cos^2(\xi)\right)\frac{\partial^2\psi}{\partial\eta^2} = \xi^{1/2}\left(\frac{\partial\Theta}{\partial\eta} - \mathtt{Nr}\frac{\partial\Phi}{\partial\eta}\right), \tag{4.15}$$

$$\left(1+a^2\cos^2(\xi)\right)\left[\frac{\partial^2\Theta}{\partial\eta^2} + \mathtt{Nb}\frac{\partial\theta}{\partial\eta}\frac{\partial\Phi}{\partial\eta} + \mathtt{Nt}\left(\frac{\partial\Theta}{\partial\eta}\right)^2\right] = \xi^{1/2}\left(\frac{\partial\psi}{\partial\eta}\frac{\partial\Theta}{\partial\eta} - \frac{\partial\psi}{\partial\xi}\frac{\partial\Theta}{\partial\eta}\right), \tag{4.16}$$

$$\left(1+a^2\cos^2(\xi)\right)\left[\frac{\partial^2\Phi}{\partial\eta^2} + \frac{\mathtt{Nt}}{\mathtt{Nb}}\frac{\partial^2\Theta}{\partial\eta^2}\right] = \mathtt{Le}\xi^{1/2}\left(\frac{\partial\psi}{\partial\eta}\frac{\partial\Phi}{\partial\xi} - \frac{\partial\psi}{\partial\xi}\frac{\partial\Phi}{\partial\eta}\right). \tag{4.17}$$

Following Narayana and Sibanda [15] we assume the transformations below

$$\hat{\eta} = \frac{\eta}{1 + a^2 \cos^2(\xi)}, \quad \psi = \xi^{1/2} f(\hat{\eta}),\ \Theta(\hat{\eta}),\ \Phi(\hat{\eta}),\ \varphi = \theta(\hat{\eta}). \tag{4.18}$$

Substituting (4.18) into (4.15) - (4.17), we will end up by the system,

$$f''' = \Theta' - \mathtt{Nr}\Phi', \tag{4.19}$$

$$\Theta'' + \frac{1}{2} f\Theta' + \mathtt{Nb}\Theta'\Phi' + \mathtt{Nt}\Theta'^2 = 0, \tag{4.20}$$

$$\Phi'' + \frac{1}{2}\mathtt{Le} f\Phi' + \frac{\mathtt{Nb}}{\mathtt{Nt}}\Theta'' = 0, \tag{4.21}$$

subject to the boundary conditions,

$$\begin{aligned} &f = 0,\ \Theta = 1,\ N_b\Phi' + N_t\Theta' = 0 \text{ on } \hat{\eta} = 0, \\ &f' \to 0,\ \Theta \to 0,\ \Phi \to 0,\ \omega = 0 \quad \text{as} \quad \hat{\eta} \to \infty. \end{aligned} \tag{4.22}$$

By using the boundary conditions (4.22) one can integrate equation (4.19) to reduce its order from the second order to the first order, hence the momentum, energy and concentration equations become

$$f' = \Theta - \mathtt{Nr}\Phi, \tag{4.23}$$

$$\Theta'' + \frac{1}{2} f\Theta' + \mathtt{Nb}\Theta'\Phi' + \mathtt{Nt}\Theta'^2 = 0, \tag{4.24}$$

$$\Phi'' + \frac{1}{2}\mathtt{Le} f\Phi' + \frac{\mathtt{Nb}}{\mathtt{Nt}}\Theta'' = 0, \tag{4.25}$$

subject to the boundary conditions,

$$\begin{aligned} &f = 0,\ \Theta = 1,\ N_b\Phi' + N_t\Theta' = 0 \text{ on } \hat{\eta} = 0, \\ &\Theta \to 0,\ \Phi \to 0. \quad \text{as} \quad \hat{\eta} \to \infty. \end{aligned} \tag{4.26}$$

.

4.3 Solution Method

In this section we will apply the spectral quasi-linearisation method to solve the governing equations (4.19)-(4.21). Before applying the SQLM, it is convenient to transform

the domain from $[0,\infty)$ into $[0,L]$ and then $[0,L]\to[-1,1]$. In the framework of the SQLM we obtain the following iteration scheme:

$$f'_{r+1}-\Theta_{r+1}+\mathrm{Nr}\Phi_{r+1}=0, \tag{4.27}$$

$$\Theta''_{r+1}+\frac{1}{2}\mathrm{Pr}\Theta' f_{r+1}+\left(\frac{1}{2}\mathrm{Pr}f_r+\mathrm{Nb}\Phi'+2\mathrm{Nt}\Theta'_r\right)\Theta'_{r+1}+\mathrm{Nb}\Theta'_r\Phi'_{r+1}=\frac{1}{2}\mathrm{Pr}f_r\Theta'_r +\mathrm{Nb}\Phi'_r\Theta'_r+\ \mathrm{Nt}\Theta'^2_r, \tag{4.28}$$

$$\frac{1}{2}\mathrm{Le}\Phi'_r f_{r+1}+\frac{\mathrm{Nt}}{\mathrm{Nb}}\Theta''_{r+1}+\Phi''_{r+1}+\frac{1}{2}\mathrm{Le}f_r\Phi'_{r+1}=\frac{1}{2}\mathrm{Le}f_r\phi'_r,, \tag{4.29}$$

Applying the Chebyshev pseudo-spectral method on (4.27) -(4.29) the SQLM scheme in matrix form is given by

$$\left[\begin{array}{c|c|c} A_{1,1} & A_{1,2} & A_{1,3} \\ \hline A_{2,1} & A_{2,2} & A_{2,3} \\ \hline A_{3,1} & A_{3,2} & A_{3,3} \end{array}\right]\left[\begin{array}{c} f_{r+1} \\ \hline \Theta_{r+1} \\ \hline \Phi_{r+1} \end{array}\right]=\left[\begin{array}{c} R_{1,r} \\ \hline R_{2,r} \\ \hline R_{3,r} \end{array}\right], \tag{4.30}$$

where f_{r+1}, Θ_{r+1}, Φ_{r+1}, $R_{1,r}$, $R_{2,r}$ and $R_{3,r}$ are vectors of size $(N+1)\times 1$ and $A_{i,j}$ are $(N+1)\times(N+1)$ matrices,

$$\begin{aligned} &A_{1,1}=\mathbf{D}, \qquad A_{1,2}=-\mathbf{I}, \qquad A_{1,3}=\mathrm{Nr}\mathbf{I},\\ &A_{2,1}=\mathbf{diag}\left[\frac{1}{2}\mathrm{Pr}\Theta'_r\right],\ A_{2,2}=\mathbf{D}^2+\mathbf{diag}\left[\frac{1}{2}\mathrm{Pr}f_r+\mathrm{Nb}\Phi'_r+2\mathrm{Nt}\Theta'_r\right]\mathbf{D},\\ &A_{2,3}=\mathbf{diag}\left[\mathrm{Nb}\Theta'_r\right]\mathbf{D},\\ &A_{3,1}=\mathbf{diag}\left[\frac{1}{2}\mathrm{Le}\Phi\right],\ A_{3,2}=\frac{\mathrm{Nt}}{\mathrm{Nb}}\mathbf{D}^2,\ A_{3,3}=\mathbf{D}^2+\mathbf{diag}\left[\frac{1}{2}\mathrm{Le}f_r\right]\mathbf{D}, \end{aligned}$$

with $\mathbf{I}$ being an identity matrix of size $(N+1)\times(N+1)$, f_{r+1}, Θ_{r+1} and Φ_{r+1} are the values of functions f, Θ and Φ at the current iteration, where f_r, Θ_r and Φ_r, are the values of functions f, Θ and Φ at the previous iteration. The initial approximation required to start the iteration process is $f(\eta)=1-e^{-\eta}$, $\Theta(\eta)=e^{-\eta}$, $\Phi(\eta)=-\frac{Nt}{Nb}e^{-\eta}$,which is a convenient random function that satisfies all the boundary conditions. To simplify the form (4.30), one can write

$$\mathbf{A}Y_{r+1}=\mathbf{R}_r \qquad , \tag{4.31}$$

where

$$\mathbf{A} = \begin{bmatrix} A_{1,1} & A_{1,2} & A_{1,3} \\ A_{2,1} & A_{2,2} & A_{2,3} \\ A_{3,1} & A_{3,2} & A_{3,3} \end{bmatrix}, \qquad Y_{r+1} = \begin{bmatrix} f_{r+1} \\ \Theta_{r+1} \\ \Phi_{r+1} \end{bmatrix}, \mathbf{R}_r = \begin{bmatrix} R_{1,r} \\ R_{2,r} \\ R_{3,r} \end{bmatrix}, \tag{4.32}$$

where A is $3\,(N+1)\times 3\,(N+1)$ square matrix while Y and R are $3\,(N+1)\times 1$. Finally the approximate solution of the system above is obtained by solving equation (4.31) as:

$$\mathrm{Y}_{r+1} = \tilde{\mathrm{A}}^{-1}\tilde{\mathrm{R}}, \tag{4.33}$$

$\tilde{\mathrm{A}}$ is the transformed matrix of A and $\tilde{\mathrm{R}}$ is the transformed vector of R after imposed the boundary conditions. The initial conditions are imposed on the first, and $(N+1)^{th}$ rows of $\mathrm{A}_{i,j}$ and $\mathrm{R}_{i,r}$. The error of the solution at each iteration r can be calculated by comparing the solutions f_r, Θ_r, Φ_r at the current iteration to the the solutions f_{r-1}, Θ_{r-1}, Φ_{r-1} at the previous iteration. We define the following relative error formula using the infinity norm

$$E_{r,N,\eta_\infty} = \frac{\|\Delta_r - \Delta_{r-1}\|_\infty}{\|\Delta_{r-1}\|_\infty} \times 100. \tag{4.34}$$

The relative error depends on the iteration r, number of grid points (which is a value chosen to be large enough to numerically approximate infinity.

4.4 Results and Discussions

The problem of laminar flow of a nano-fluid due to a wavy surface has been analyzed. We used spectral quasi-linearisation scheme to solve the governing equations. The accuracy of the method and the effects of some physical parameters shown in tabular and graphically. Fig. 4.1 shows the effects of buoyancy parameter Nr on the velocity profile. With an increase in fluid buoyancy the velocity decreases. Fig. 4.2 illustrates effects of thermophoresis and Brownian motion parameters on the velocity profile respectively. It is clear that increasing Brownian motion tends to enhancement

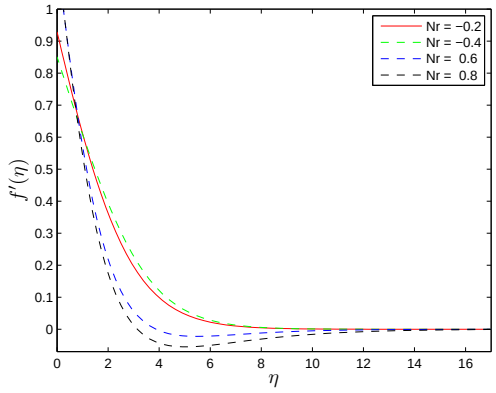

Figure 4.1: Effect of the buoyancy ratio parameter Nr on the velocity of the fluid for $Nb = 0.6$, $Nt = 0.3$, and $Le = 1$.

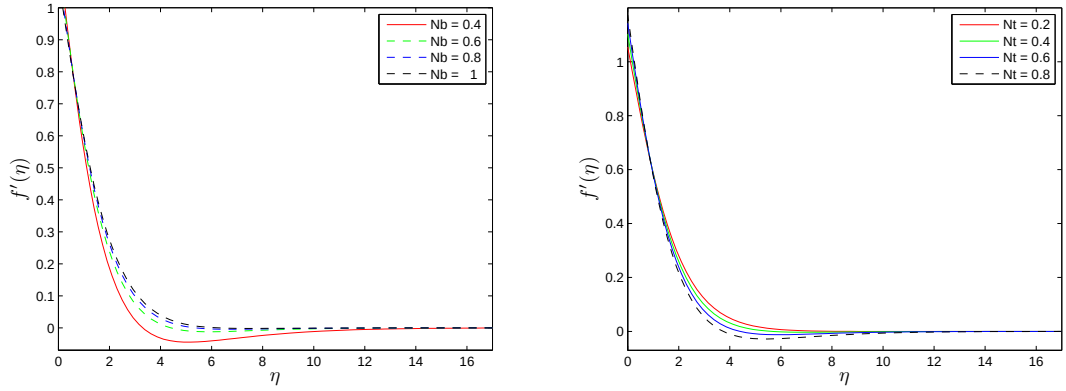

(a) The Velocity profile

(b) The Velocity profile

Figure 4.2: Effect of the Nb and Nt on $f'(\eta)$for $Nr = 0.5$, $Nb = 0.6$, $Le = 1$ and $Nt = 0.3$.

in the velocity profile. On the other hand the opposite result will be obtained by increasing the thermophoresis. The temperature and the volume fraction are plotted in Fig. 4.2(a) and (b) for different values of the buoyancy parameter Nr. Fig. 4.3(a)

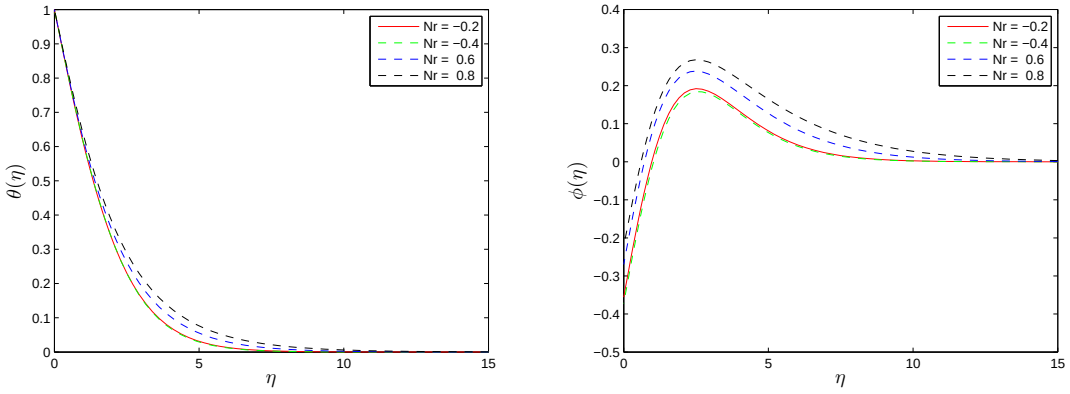

(a) Temperature profile (b) Concentration profile

Figure 4.3: Effect of Nr on $\theta(\eta)$ and $\phi(\eta)$ respectively for $a = 0.8$, $Nb = 0.6$, $Le = 1$ and $Nt = 0.3$.

and (b) display the variations of the dimensionless temperature $\theta(\eta)$ and mass volume fraction for different values of Nr. It is clear that the temperature profile increases with increasing values of Nr. On the other hand, the mass volume fraction profile in boundary layer decreases with an increase in Nr. Effect of the thermophoresis parameter Nt on both temperature mass volume fraction profiles has been plotted in Fig. 4.4. The thermophoresis force generated by the temperature gradient creates a fast flow away from the stretching surface. In this way more fluid is heated away from the surface, and consequently, as Nt increases, the temperature within the boundary layer increases. The fast flow from the stretching sheet carries with it nanoparticles leading to an increase in the mass volume fraction boundary layer thickness. The effect of the random motion of the nanoparticles suspended in the fluid on the temperature and nanoparticle volume fraction is shown in Fig. 4.5(a) and (b). As expected, the increased Brownian motion of the nanoparticles carries with it heat and the thickness of the thermal boundary layer increases. The Brownian motion of the nanoparticles

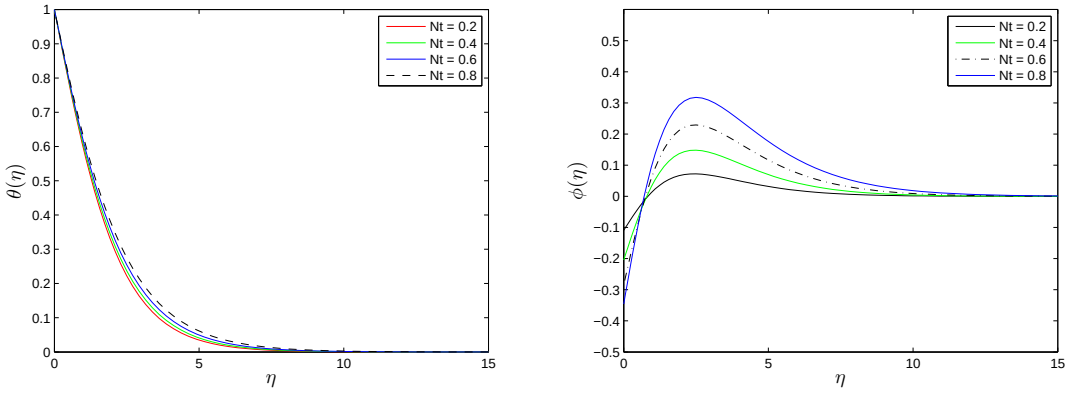

(a) Temperature profile (b) Concentration profile

Figure 4.4: Effect of the amplitude of Nt on $\theta(\eta)$ and $\phi(\eta)$ respectively for $Nr = 0.5$, $Nb = 0.6$, $Le = 1$ and $a = 0.8$.

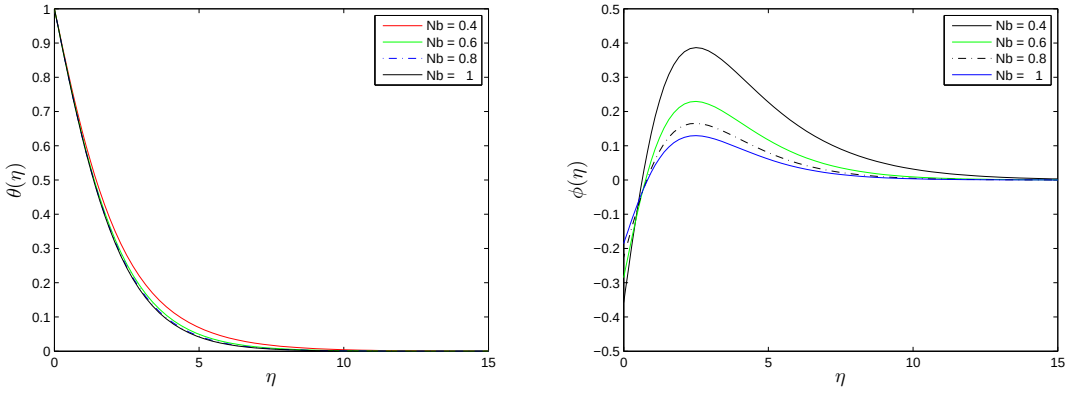

(a) Temperature profile (b) Concentration profile

Figure 4.5: Effect of Nb on $\theta(\eta)$ and $\phi(\eta)$ respectively for $Nr = 0.5$, $a = 0.8$, $Le = 1$ and $Nt = 0.3$.

increases thermal transport which is an important mechanism for the enhancement of thermal conductivity of nanofluids. However, we note that increasing the Brownian motion parameter leads to a clustering of the nanoparticles near the stretching sheet. An increase in the Brownian motion of the nanoparticles leads to a decrease in the mass volume fraction profiles. The axial distribution of the heat and mass volume

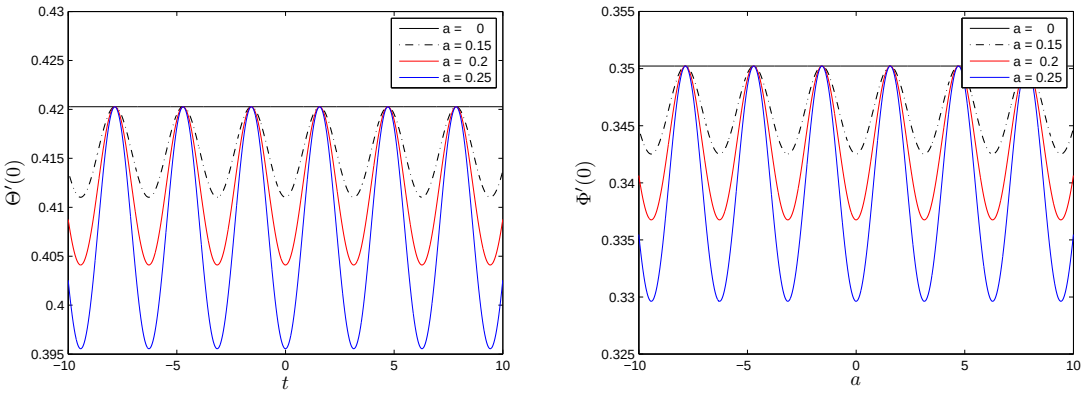

(a) The rate of heat transfer (b) The rate of Nano-mass transfer

Figure 4.6: Effect of the amplitude of the surface wave a on $-\Theta'(0)$ and $-\Phi'(0)$ respectively for $Nr = 0.5$, $Nb = 0.6$, $Le = 1$ and $Nt = 0.3$.

fraction transfer coefficients for several values of a are shown in Fig. 4.6 respectively. We observed that, increasing a decreased both the heat and volume fraction transfer coefficients. Fig. 4.7 shows effect of the thermophoresis parameter on both the rate of heat and mass volume fraction transfer coefficients respectively. We observe that an increase in Nt leads to decrease of the rate of heat transfer coefficient, while the mass transfer coefficient is relatively sensitive and strongly influenced by the changes in the thermophoresis parameter.

Fig. 4.8 gives the details of the variation of both the rate of heat and mass volume fraction transfer coefficients, respectively, for different values of the Brownian motion Nb. It is clear that an increase in Nb leads to a considerable thinning of the thermal boundary layer, and thus a reduction in rate of heat transfer. From the same figure it is evident that as Nb increases, the mass volume fraction boundary layer thickness

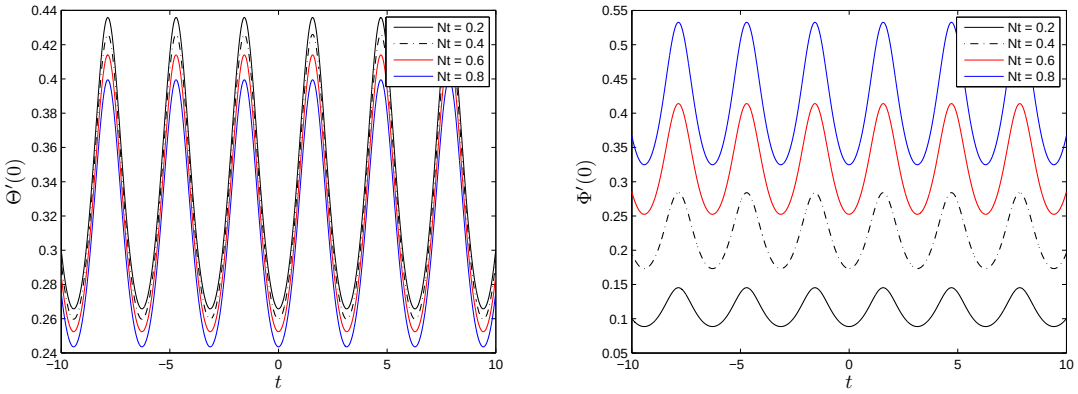

(a) The rate of heat transfer (b) The rate of Nano-mass transfer

Figure 4.7: Effect of the thermophoresis parameter Nt on $-\Theta'(0)$ and $-\Phi'(0)$ respectively for $Nr = 0.5,\ Nb = 0.6,\ Le = 1$ and $a = 0.8$.

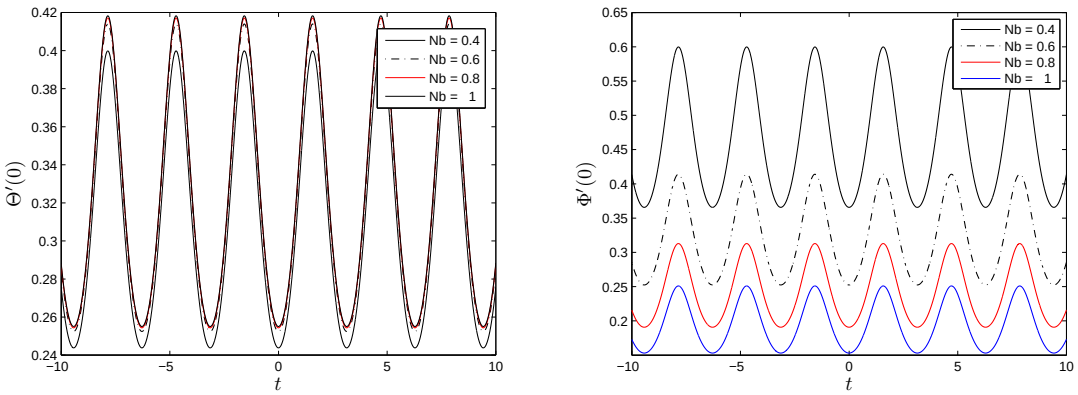

(a) The rate of heat transfer (b) The rate of Nano-mass transfer

Figure 4.8: Effect of the Brownian motion parameter Nb on $-\Theta'(0)$ and $-\Phi'(0)$ respectively for $Nr = 0.5,\ Nt = 0.6,\ Le = 1$ and $a = 0.8$.

increases causing a enchantment in the Sherwood number.

Chapter 5

conclusions

We outline the main findings in each chapter and highlight some of the general results that were found and the conclusions that have been drawn from this work. To solve the nonlinear equations governed the Convective heat transfer over inverted Cone we used spectral quasi-linearisation method. The solution obtained through the use of the SQLM compared with those in the literature review to determine the accuracy and computational efficiency. We also determined the effect of the power-law index parameter on the fluid properties graphically. Also we studied the nano-fluid flow over a wavy surface with non-controllable nanoparticle flux at the boundary. The governing equations were solved using the SQLM. The effects of the governing parameters have been presented graphically. We found that increase in the thermophoresis parameter leads to decrease of the rate of heat transfer coefficient, while the mass transfer coefficient is relatively sensitive and strongly influenced by the changes in the thermophoresis parameter. Increase in the Brownian motion parameter leads to a considerable thinning of the thermal boundary layer, and thus a reduction in rate of heat transfer. From the previous mentioned it is evident that as the Brownian motion parameter increases, the mass volume fraction boundary layer thickness increases causing a enchantment in the Sherwood number.

Bibliography

[1] A. Aziz, W.A. Khan, I. Pop, *Free convection boundary layer flow past a horizontal flat plate embedded in porous medium filled by nanofluid containing gyrotactic microorganisms*, Inter. Journal of Thermal Sciences, 56 (2012) 48-57.

[2] R. E. Bellman and R. E. Kalaba, *Quasilinearization and Nonlinear Boundary-Value problems*, Elsevier Publishing Company,New York,1965

[3] D. Samuel Conte and Carl de Boor, *Elementary numerical analysis*, McGrow Hill International Editions,1981 .

[4] C. Canuto, M.Y. Hussaini, A. Quarteroni, and T.A. Zang, *Spectral Methods in fluid dynamics*, Springer-Verlag, Berlin, 1988.

[5] A. Chamkha, R.S.R Gorla, K. Ghodeswar,*Non-similar solution for natural convective boundary layer flow over a sphere embedded in a porous medium saturated with a nanofluid.* Transport in Porous Media, 86 (2011) 13-22.

[6] C.Y. Cheng,*Free convection boundary layer flow over a horizontal cylinder of elliptic cross section in porus media saturated by a nanofluid, International Communications in Heat and mass Transfer*, 39 (2012) 931-936.

[7] SUS. Choi *Enhancing thermal conductivity of fluid with nanoparticles, developments and applications of non-Newtonian flows.* FED 23 (1995) 99-105.

[8] SUS. Choi, Zhang ZG, Yu W, Lockwood FE, Grulke EA: *Anomalously thermal conductivity enhancement in nanotube suspensions.* Appl. Phys. Lett, 79 (2001) 2252-2254

[9] J. Eapen, R. Rusconi, R. Piazza, S. Yip, *The classical nature of thermal conduction in nanofuids*. ASME J. Heat Transfer,132 (2010) 102402.

[10] J. Fan, L. Wang, *Effective thermal conductivity of nanofuids: the effects of microstructure*. J. Phys. D A- Appl. Phys., 43 (2010) 165501.

[11] S. Kakac, A. Pramuanjaroenkij, *Review of convective heat transfer enhancement with nanofluid. International Journal of Heat and Mass Transfer* 52 (2009) 3187-3196.

[12] R. Krivec and V. B. Mandelzweig, *Numerical investigation of quasilinearization method in quantum mechanics*, Computer Physics Communications, 138, 69(2001).

[13] R. Kalaba, *On nonlinear differential equation, the maximum operation and monotone convergence*, J. Math. Mech. 8,519(1959).

[14] V. Lakshmikantham and A. S. Vatsala, *Generalized Quasilinearizationor Nonlinear problems*, mathematics and its applications, Volume 440, Academic Publishers, Dordrecht,1998.

[15] P.A. Lakshmi Narayana and P. Siband, Soret and Dufour effects on free convection along a vertical wavy surface in a fluid saturated Darcy porous medium, International Journal of Heat and Mass Transfer. 53 (2010) 3030 - 3034.

[16] V. B. Mandelzweig, *Quasilinearization method and its verification on exactly solvable models in quantum mechanics*, J. Math. Phys. 40,6266 (1999).

[17] H. Masuda, A. Ebata, K. Teramae, N. Hishinuma, *Alteration of thermal conductivity and viscosity of liquid by dispersing ultra-fine particles*. Netsu Bussei,5 (1993) 227-233.

[18] S.S Motsa and P. Sibanda (2013). *On extending the quasilinearization method to higher order convergent hybrid schemes using the spectral homotopy analysis method*. Journal of Applied Mathematiics.vol.2013,Article ID 879195, 9 pages, 2013.doi:10.1155/2013/879195.

[19] D.A. Nield, A.V. Kuznetsov, *The Cheng-Minkowycz problem for natural convective boundary-layer flow over a porous medium saturated by a nanofluid*, International Journal of Heat and Mass Transfer, 52 (2010) 5792-5795.

[20] D.A. Nield, A.V. Kuznetsov, *Thermal instability in a porous medium layer saturated by a nanofluid*: Brinkman model. Transport in Porous Media, 81 (2010) 409-422.

[21] A. Ralson and P. Rabinowitz, *A first course in numerical analysis*, McGrow Hill International Editions,1988

[22] D.A.S. Rees, I. Pop, Free convection induced by a horizontal wavy surface in a porous medium, Fluid Dyn. Res. 14 (1994) 151-166.

[23] A.R.Sohouli, M. Famouri, A. Kimiaeifar, G. Domairry *Application of homotopy analysis method for natural convection of Darcian fluid about avertical full cone embedded in pours media prescribed surface heat flux*, J. Commun Nonlinear Sci Numer Simulat 15(2010)1691-1699.

[24] L. N. Trefethen, *Spectral Methods in MATLAB*, SIAM, 2000